Materials and Design 30 (2009) 4012–4022

Contents lists available at ScienceDirect

Materials and Design

journal homepage: www.elsevier.com/locate/matdes

The application of shoulderless conical tools in friction stir welding: An experimental and theoretical study

D.H. Lammlein *, D.R. DeLapp, P.A. Fleming, A.M. Strauss, G.E. Cook

Vanderbilt University, Welding Automation Lab, Nashville, TN 37235, United States

ARTICLE INFO

Article history:
Received 5 February 2009
Accepted 14 May 2009
Available online 21 May 2009

Keywords:
Friction stir welding
Conical probe
Aluminum
Butt-joints

ABSTRACT

A friction stir welding (FSW) tool geometry, consisting of a shoulderless conical probe, is investigated for application to closed contour welding, variable thickness welding, and open-loop control welding. By use of a tapered retraction procedure and a ramped rotational velocity, a conical tool may facilitate material disengagement with minimal surface defects in applications which do not permit weld termination defects (e.g. pipes, pressure vessels, fuselages, nosecones). In addition, because the vertical position of the tool relative to the material surface is less critical with a conical tool than with other tool designs, it can be used in a open-loop fashion (i.e. without process force feedback control) and on materials whose thicknesses are highly variable. The use of a conical probe without a shoulder is not documented in the literature and it is the aim of this work to establish the conditions for mechanically sound welds. Effective tool geometries and process variables are found via experimental analysis. Thermal, tensile, macrosection, and process force data are presented along with a computational fluid dynamics (CFD) process model. It is concluded that this type of tooling is capable of producing acceptable welds when applied to butted aluminum plates and that similar methods would likely be effective in the applications described previously.

1. Introduction

The conical tool design is potentially a simple solution to the problem of closure in friction stir welding (FSW). According to Trapp, Fischer, and Bernath of the Edison Welding Institute (ESI) in US Patent #7,234,626, the appropriate conical inclusive angle can contain weld material regardless of cone penetration depth and during tapered retraction [1,2]. The conical tool, Fig. 1, in conjunction with the tapered retraction procedure and spindle velocity ramping could therefore be used to weld closed contours such as cylinders and spheres (e.g. pipes, pressure vessels, fuselages, nosecones) without leaving a defect or hole where the tool exits the material. The conical tool design is especially attractive because it is an easily manufacturable and durable design. The conical tool is potentially a simple and elegant solution to the seemingly complex problem closure welding in FSW. A current solution to the retraction problem that NASA and a number of manufacturers have adopted is an exceedingly complex, hydraulically actuated retractable pin tool apparatus [3]. The conical tool can be used for in-process adjustment of penetration depth (i.e. variable thickness welds). Additionally, the use of a conical tool does not require force control as with a conventional friction stir weld tool where appropriate shoulder contact with the material is critical. These welds can be performed in an open-loop manner without process force feedback based adjustment of the tool's vertical position. The conical tool can passively accommodate variation in the height of the material surface relative to the tool, due to material thickness variations in linear welds or system eccentricities in rotary welds.

As no published literature exists on the design and application of shoulderless conical tools, the primary aim of this work is to find a tool geometry and weld parameter set which produces mechanically acceptable welds. An experimental weld matrix has been performed on 1/8 in. (0.32 cm) thick, butted 6061 alloy aluminum plates. A suitable inclusive angle for FSW was found by testing a range of tool angles (60°, 80°, 90°, and 120°). Suitable weld parameters were established and a 36 weld matrix was performed with the 80° and 90° tools. For these welds, characteristic weld forces were determined via a dynamometer, achievable weld strengths via tensile testing, weld structure and appearance via etching of macrosections, and approximate shoulder edge temperature via thermal camera images. To avoid both collision of the tool with the backing anvil and weld root defect formation, a penetration ligament of 0.01 in. (0.25 mm) was selected for the experiment.

Welds made at a low spindle head angle (0–2°) resulted in unacceptable force oscillations in the *XY* plane. Fig. 2 shows the

* Corresponding author. Tel.: +1 615 3223322.
E-mail address: d.lammlein@vanderbilt.edu (D.H. Lammlein).

0261-3069/$ - see front matter © 2009 Elsevier Ltd. All rights reserved.
doi:10.1016/j.matdes.2009.05.023

XY plane oscillations in the dynamometer force data for a particular weld at 0° spindle head angle. The experiment was therefore conducted at a head angle off 4° where the problem did not arise. The oscillations at low spindle head angles can be

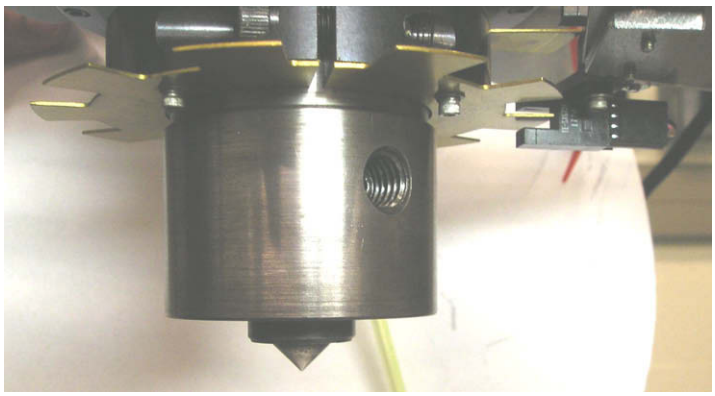

Fig. 1. A shoulder-less, conical tool (90° inclusive angle) used in the experiment.

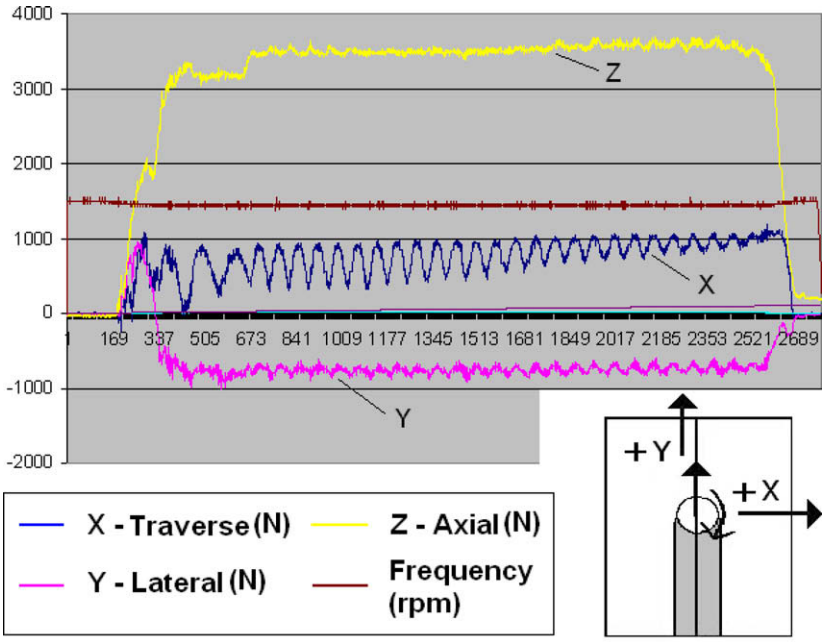

Fig. 2. *XY* plane force oscillations were typically present at low spindle head angles with conical welds, presumably due to the lack a horizontal, stabilizing shoulder. The experiment was therefore performed at a 4° angle where this problem did not exist.

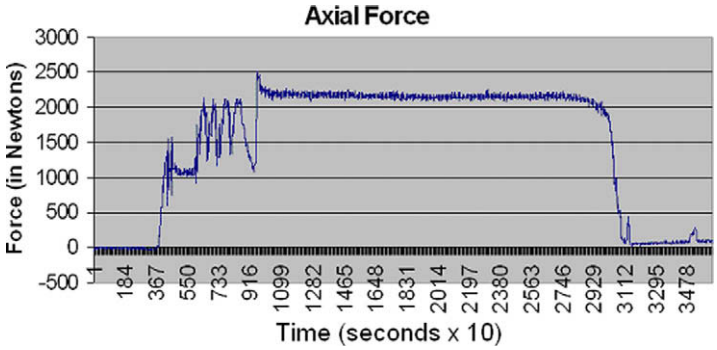

Fig. 3. Typical axial (*Z*-axis) force data.

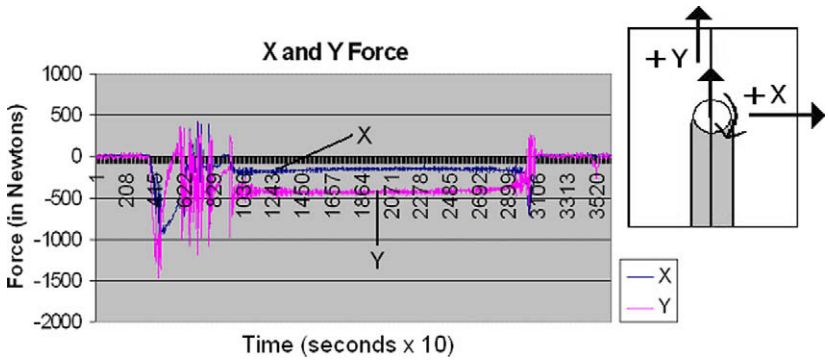

Fig. 4. Typical in-plane force data.

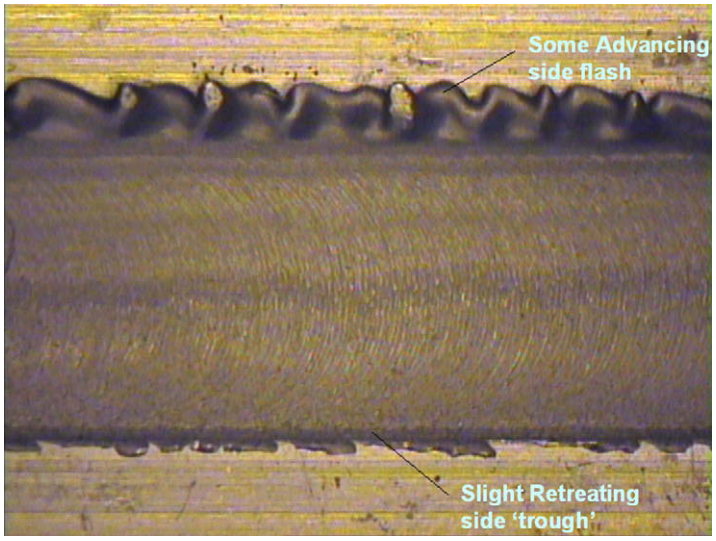

Fig. 5. Typical surface appearance for 90° conical tool welds on 1/8 in. thick butted 6061 alloy aluminum plates. Typical conical surface defects are pointed out.

attributed to physical tool deflection and a lack of stiffness in the experimental setup. This problem is not perceptible with conventional tooling and it must therefore be concluded that the conical tool geometry exacerbates *XY* plane tool deflection and induces force oscillations. The lack of the stabilizing influence of a horizontal shoulder on the material surface is believed to contribute to this deflection. In addition, as compared to conventional tooling, the dynamometer data showed axial (Z) forces, Fig. 3, that were lower in magnitude relative to the *XY* plane forces, Fig. 4. The result of this periodic tool deflection was a coarse surface banding as opposed to a fine surface finish. The problem is alleviated at a 4° spindle head angle.

2. Results and discussion

2.1. Experimental analysis

The 80° and 90° conical tools were selected for the experimental weld matrix because they produced the highest quality welds based on surface appearance. Conical welds typically produced advancing side flash and a trough-like surface defect on the retreating side, Fig. 5. These defects were reduced to acceptable levels using the 80° and 90° conical inclusive angle tools. Macrosections were made for each weld using Boss's reagent for etching. A complete table of macrosections is included in Fig. 6a–h. Despite a similar superficial appearance and similar weld macrosections, welds made with the 80° tool were vastly inferior in strength, Fig. 7a and b, to those made with the 90° tool at all parameter values and for all runs. Welds made with the 80° tool do however show a pronounced, crack-like defect extending from the root of the weld to the weld nugget center. This defect is less pronounced or absent in the 90° weld macrosections. Typical process forces for this tool type are lower in magnitude to those of a similar conventional weld, Fig. 8a–h. The ratio of in-plane force to axial force (i.e. $\sqrt{(x^2+y^2)}/z$) is however higher for this process which is believed to increase vibration and process instability.

The thermal camera was calibrated to the emissivity of the conical tool surface. The weld temperatures listed in Fig. 9a and b were calculated by taking the average temperature from a rectangular area on the tool surface just above the weld material surface at increments in time. Ten images at 1 s intervals were used from the thermal camera video and those were then averaged to produce an approximation of the temperature on the cone surface during the steady-state portion of the weld. It should be noted that the temperature continued to creep upward even during the steady state period. In addition, welds made later in the day (when the machine, fixturing, and backing plate were warm) were noticeably warmer (as much as 20 °C).

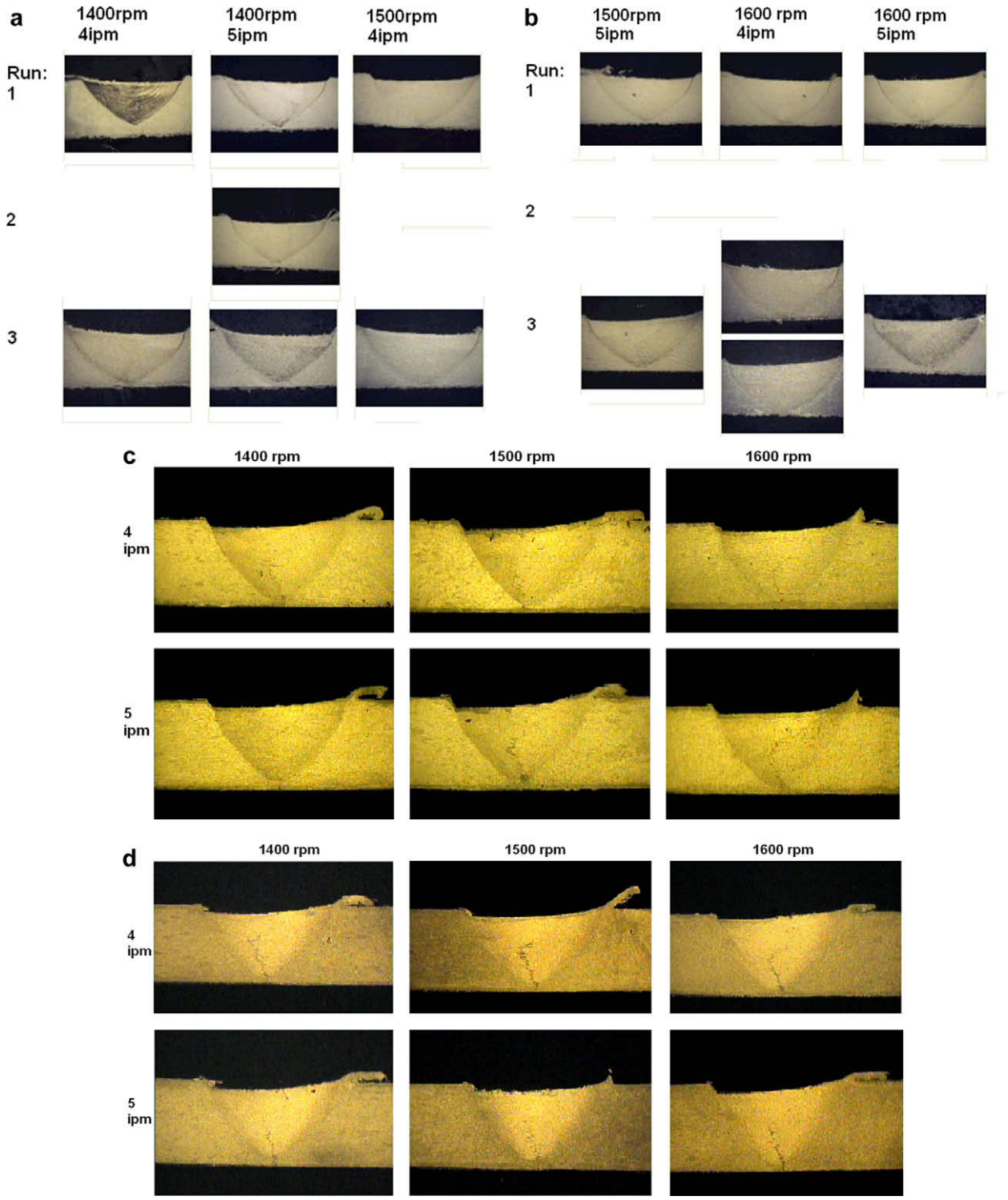

Fig. 6. (a) 90° conical tool macrosections. Table of experimental macrosections (80° and 90° tools). Some 90°, Run2 welds were not macrosectioned and one weld was macrosectioned twice (90°,1600 rpm, 4 ipm, Run3), (b) 90° conical tool macrosections. *Note*: Run3, 1600 rpm, 4 ipm, 90° was macrosectioned twice. Table of experimental macrosections (80° and 90° tools). Some 90°, Run2 welds were not macrosectioned and one weld was macrosectioned twice (90°,1600 rpm, 4 ipm, Run3), (c) Run1, 80° conical tool macrosections. Table of experimental macrosections (80° and 90° tools). Some 90°, Run2 welds were not macrosectioned and one weld was macrosectioned twice (90°, 1600 rpm, 4 ipm, Run3), (d) Run2, 80° conical tool macrosections. Table of experimental macrosections (80° and 90° tools). Some 90°, Run2 welds were not macrosectioned and one weld was macrosectioned twice (90°, 1600 rpm, 4 ipm, Run3), (e) Run3, 80° conical tool macrosections. Table of experimental macrosections (80° and 90° tools). Some 90°, Run2 welds were not macrosectioned and one weld was macrosectioned twice (90°, 1600 rpm, 4 ipm, Run3), (f) macrosection of the strongest conical weld (90°, 1600 rpm, 4 ipm, Run#1). A minimal penetration ligament is crucial to weld strength. Failure in the tensile coupon occurred along the retreating (right) side weld nugget boundary, (g) macrosection of the weakest 90° conical weld (90°, 1400 rpm, 4 ipm, Run#1). Failure occurred at the jointline and along the retreating side weld nugget boundary. A significant lack of penetration (weld root) defect can be seen in this weld indicating a slight error in the automated zeroing process for this particular weld. Three welds at each parameter set were performed to distinguish such outliers, (h) a particularly revealing macrosection (90°, 1400 rpm, 5 ipm, Run#1). A jointline remnant can be seen curving through the weld nugget center. In addition, the lack of consolidation near the cone tip which is typical of a cone weld can be seen clearly here. The lack of sufficient probe surface area, heating, and pressure at the cone tip result in a lack of consolidation there.

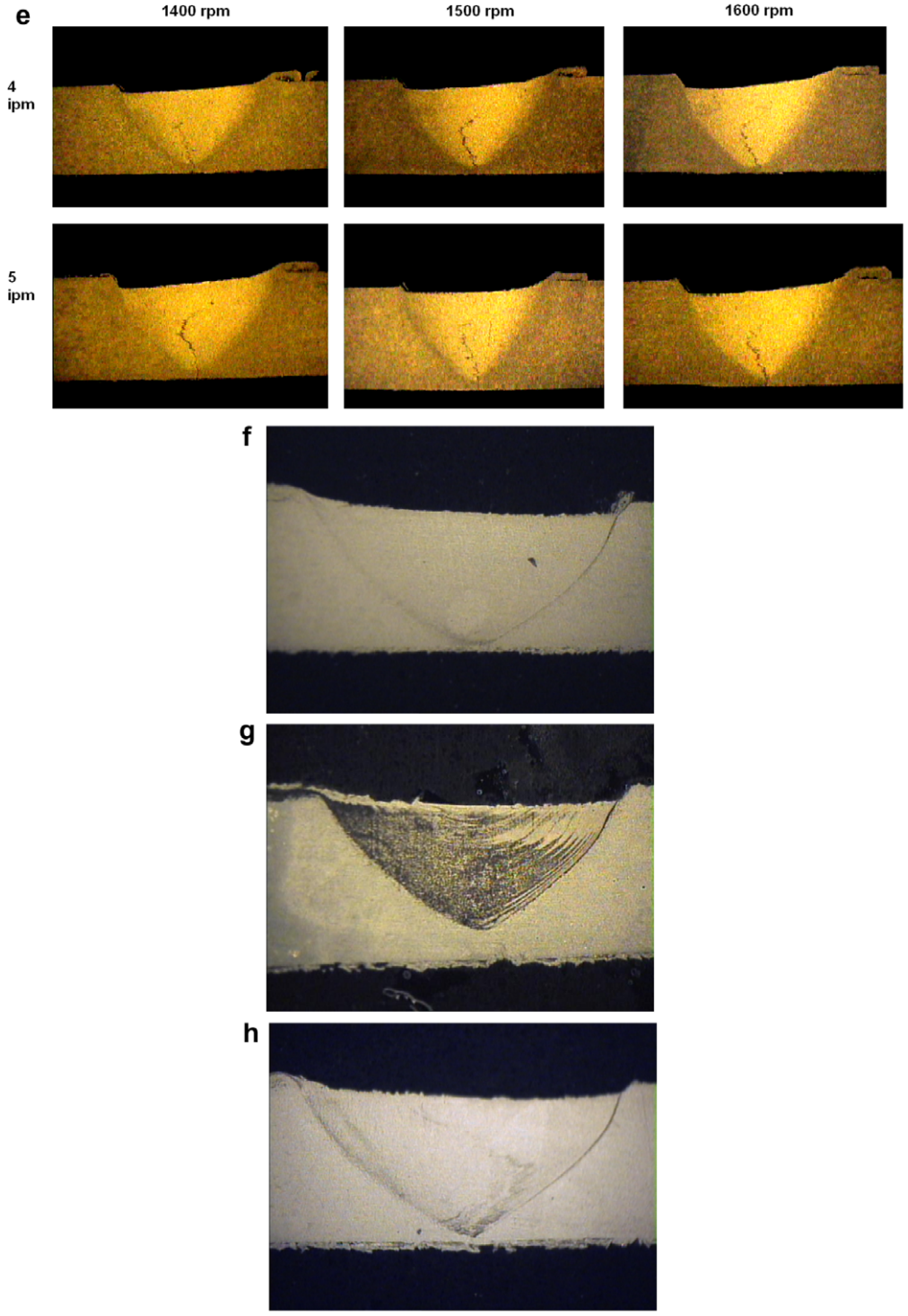

Fig 6. *(continued)*

2.2. CFD model of conical tool FSW

The Eularian, finite volume, CFD solver, Ansys FLUENT was used with the implicit formulation. The weld material viscosity function was set by user-defined function and defined according to the visco-plastic model of Sheppard and Wright [4], Eq. (1), as modified from the initial formulation proposed by Sellars and Tegart [5]. Flow stress is defined as an inverse hyperbolic sine function of the local strain rate magnitude and absolute temperature in this following commonly used form:

$$Z = \dot{\varepsilon} \exp\left(\frac{Q}{RT}\right) = A(\sin \alpha \sigma_e)^n \tag{1}$$

or equivalently,

$$\sigma_e = \frac{1}{\alpha} \sinh^{-1}\left[\left(\frac{Z}{A}\right)^{\frac{1}{n}}\right], \quad Z = \dot{\varepsilon} \exp\left(\frac{Q}{RT}\right)$$

where α, A, n are material constants ($\alpha = 0.045$ (MPa^{-1}), $Q = 145$ kJ mol^{-1}, $A = 8.8632\text{E}6$ s^{-1}, $n = 3.55$), σ_e is the equivalent

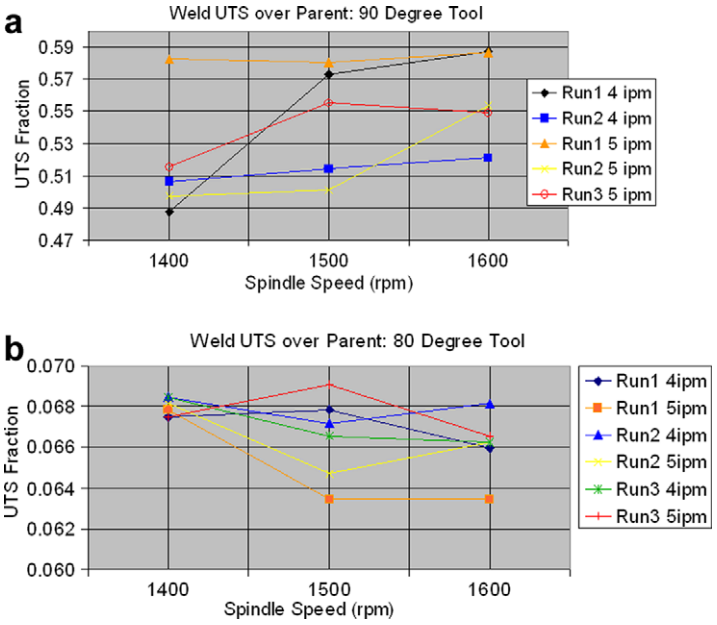

Fig. 7. (a) (90° tool) Ultimate tensile strength of weld specimen over that of the parent plotted against spindle speed in rpm. Three welds were performed at each parameter set (ipm, rpm) and (b) (80° tool) Ultimate tensile strength of weld specimen over that of the parent plotted against spindle speed in rpm. Three welds were performed at each parameter set (ipm, rpm).

steady state flow stress (MPa), R the gas constant ($R = 8.314\ \text{mol}^{-1}\ \text{K}^{-1}$), T the absolute temperature (K), Q the activation energy (J mol^{-1}), and Z the Zener–Hollomon parameter. The material constants used are determined using a hot compression test. The material viscosity is defined in the following manner:

$$\mu = \frac{\sigma_e}{3\dot{\varepsilon}} \tag{2}$$

The visco-plastic model, Eq. (2), is valid at temperatures reasonably below the metal's solidus temperature. As the material approaches the solidus temperature significant softening occurs. The total heat input was calculated via the weld power method [6–14]:

$$P = \omega \cdot M \tag{3}$$

$$Q = P \cdot \beta \tag{4}$$

where P, Eq. (3), is the weld power (W), Q is the heat input to the tool and weld material (W), ω is the tool rotational speed (rad/s), M is the measured torque (N m), and β is the fraction of mechanical work dissipated as heat into the tool shank and the weld. Chao and Qi [15] arrive at a β value, Eq. (4), of approximately 0.8 under similar conditions using a boundary value approach and determine that approximately 5% of this dissipated heat is dissipated via the tool shank. Those ratios are found to be reasonable in the current study. The weld moment was found experimentally by means of a rotating cutting force dynamometer and the spindle speed setting was verified by optical interrupters. This calculated total heat input was then applied in the model at the tool-material interface via a user-defined function which varies heat input over the tool surface according to the local tangential velocity magnitude. Heat input is therefore highest near the tool shoulder edge and zero at the center of the probe tip with the total heat input equal to the weld power. Heat input to the tool shank is determined by imposing the local weld material temperature at the interface onto the corresponding local tool surface element via a user-defined function. A variable slip shear condition was set at the weld interface [16]. The tool rotational velocity was set to 70% of the experimental parameter and a pure stick condition was used. This simple boundary condition was used because the actual relationship is unknown and unwarranted complexity is not desired in the model.

The CFD model geometry consisting of 510,299 tetrahedral elements can be seen in Fig. 10. The tool traverse was imposed in the model by leaving the tool at the model origin and establishing a velocity inlet and pressure outlet for the aluminum plate. Fig. 11 shows the increasing element refinement towards the weld interface. The thermal boundary conditions used in the model are shown in Fig. 12. The resulting temperature gradients can also be seen. Fig. 13 shows the temperature gradients in the vicinity of the weld interface. Fig. 14 is a lateral cross-section view of the weld model showing contours of velocity magnitude in the material surrounding the tool. This type of graph outlines the thermomechanically affected zone (TMAZ). The model shows a lack of stirring at the tip of the conical probe. This agreed with experimental observations in the weld macrosections and in the manner of tensile coupon failure. Porosity, lack of consolidation, and crack-like defects can be seen in some of the macrosections, particularly those from weaker weld runs. In addition, the line of failure in tensile samples intersected the weld root in almost all cases, indicating weakness near the probe's tip as indicated by the lack of stirring seen in the CFD model.

3. Conclusions

The conical tool reduces the process forces drastically (particularly the vertical). In this experiment the 90° tool welds retained a reasonable percentage of parent material strength (50–60%). The lack of the stabilizing influence of the shoulder results in increased tool deflection in XY plane but the difficulty can be alleviated with a large (4° here) spindle head angle. Weld line following was found to be more critical with a conical tool because the decreasing diameter of the cone near its tip leaves little room for tool to weld line alignment errors. This sort of lateral misalignment will result in a so-called weld root defect.

The 90° tool was shown to work better than the 60°, 80°, or 120° tools. Small cone inclusive angles require higher spindle speeds

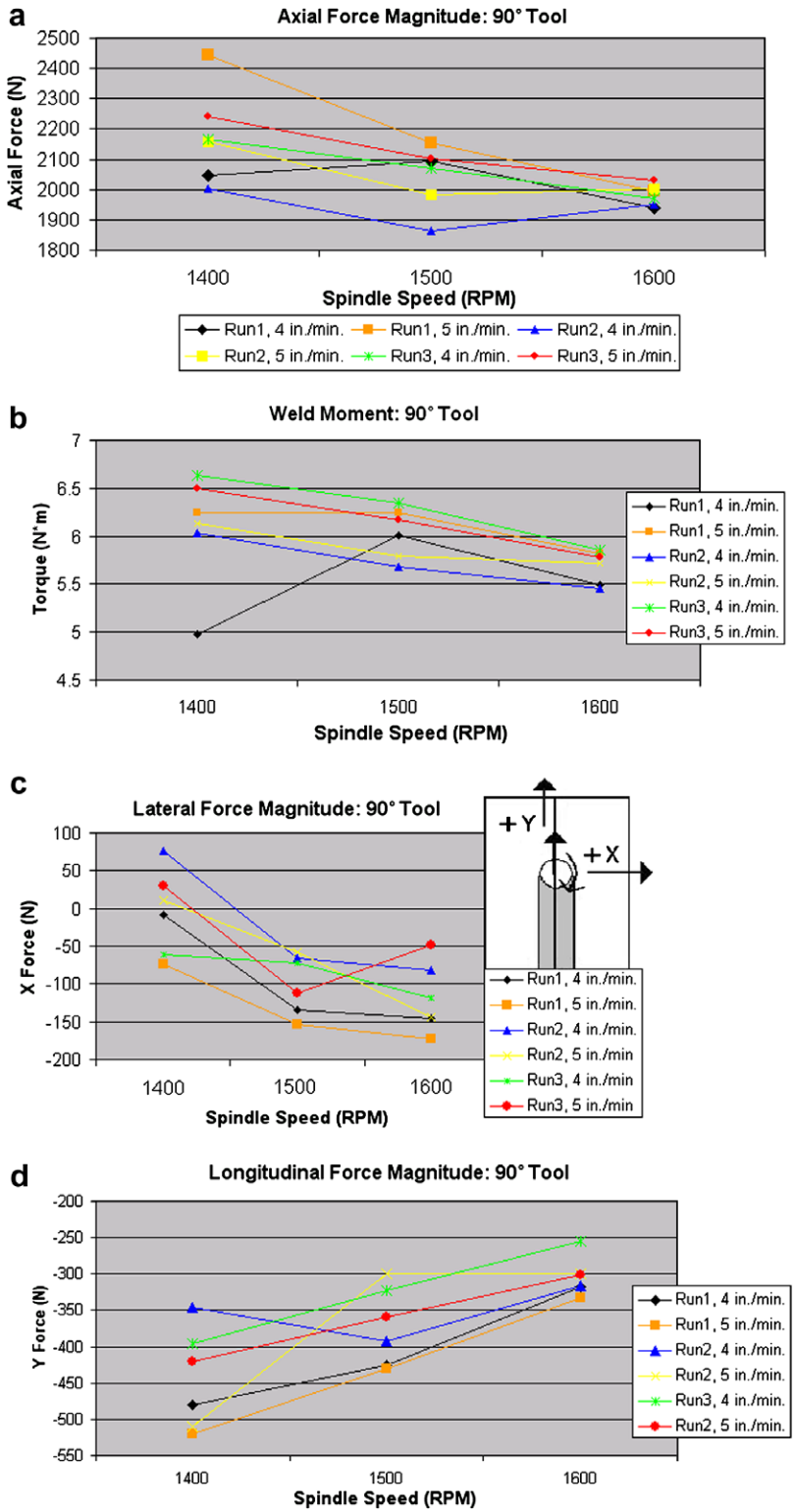

Fig. 8. (a) (90° tool) Axial force magnitude for each weld plotted against spindle speed in rpm. Three welds were performed at each parameter set (ipm, rpm). 8000 N is typical for a similar conventional weld (3/4 in. dia. shoulder, ½ in.–20 pin). Conical welds produce significantly lower axial force, (b) (90° tool) Weld moment for each weld plotted against spindle speed in rpm. Three welds were performed at each parameter set (ipm, rpm). 18 N m is typical for a similar conventional weld (3/4 in. dia. shoulder, ½ in.–20 pin). Conical welds produce significantly lower weld moment, (c) (90° tool) Lateral force magnitude for each weld plotted against spindle speed in rpm. Three welds were performed at each parameter set (ipm, rpm). +2500 N *Y* is typical for a similar conventional weld (3/4 in. dia. shoulder, ½ in.–20 pin). Conical welds produce significantly lower lateral force (change in sign due to clockwise vs. counter-clockwise rotation), (d) (90° tool) Longitudinal force magnitude for each weld plotted against spindle speed in rpm. Three welds were performed at each parameter set (ipm, rpm). +2500 N *X* is typical for a similar conventional weld (3/4 in. dia. shoulder, ½ in.–20 pin). Conical welds produce significantly lower longitudinal force. Sign for a particular weld is dependent to clockwise vs. counter-clockwise rotation. All conical welds in this experiment were made with clockwise rotation, (e) (80° tool) Axial force magnitude for each weld plotted against spindle speed in rpm, (f) (80° tool) Weld moment for each weld plotted against spindle speed in rpm, (g) (80° tool) Lateral force magnitude for each weld plotted against spindle speed in rpm, (h) (80° tool) Longitudinal force magnitude for each weld plotted against spindle speed in rpm.

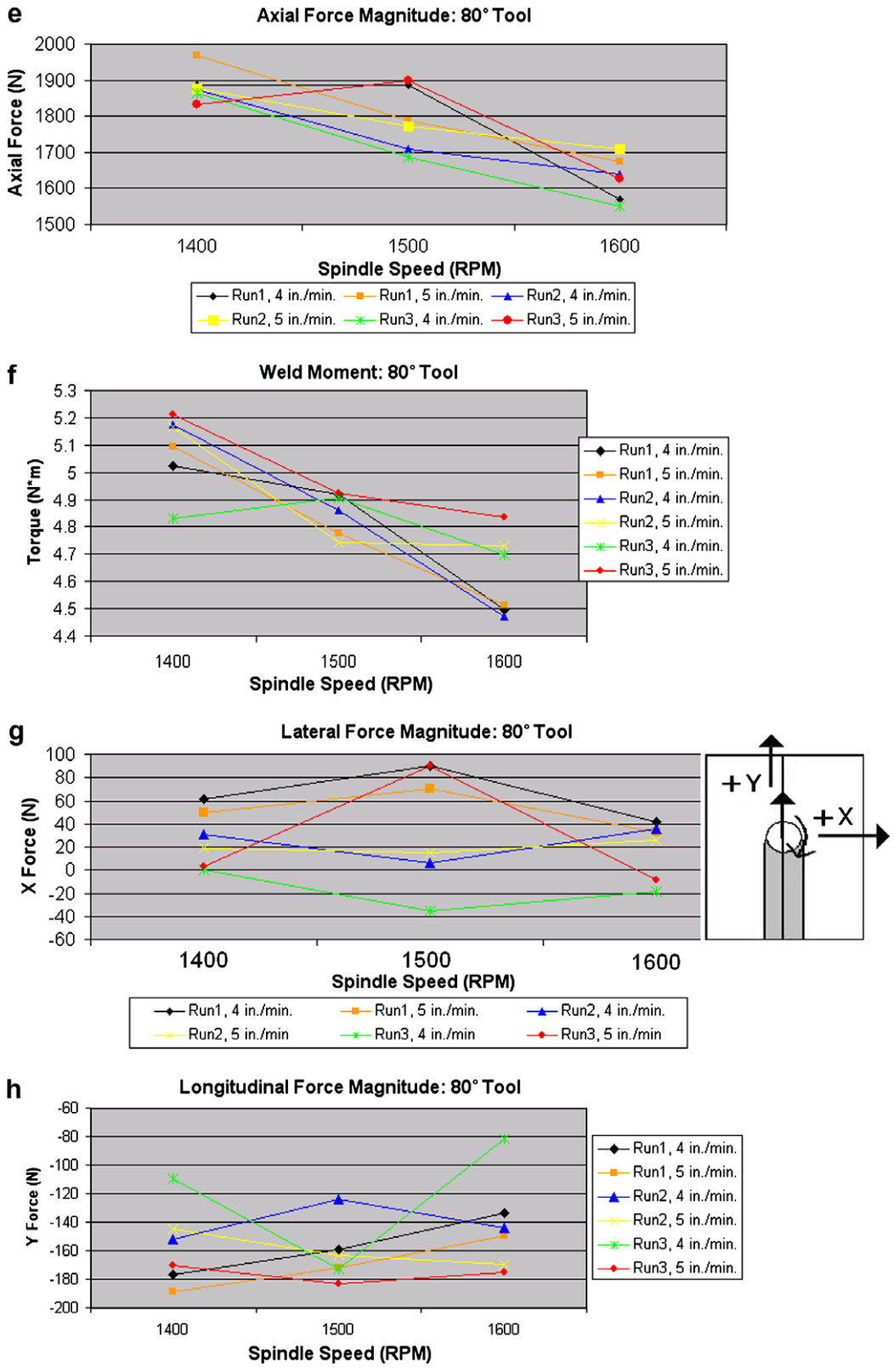

Fig 8. *(continued)*

and create more flash while large angles produce larger processed and heat affected zones. Failures typically occurred at the jointline (appropriate penetration ligament and jointline following are critical) and along the retreating side boundary of the weld nugget where a lack of consolidation (dark line) could sometimes be seen in macrosections.

Full probe tapered retraction proved to be difficult. Pictured in Fig. 15 are some preliminary attempts at this using various retrac-

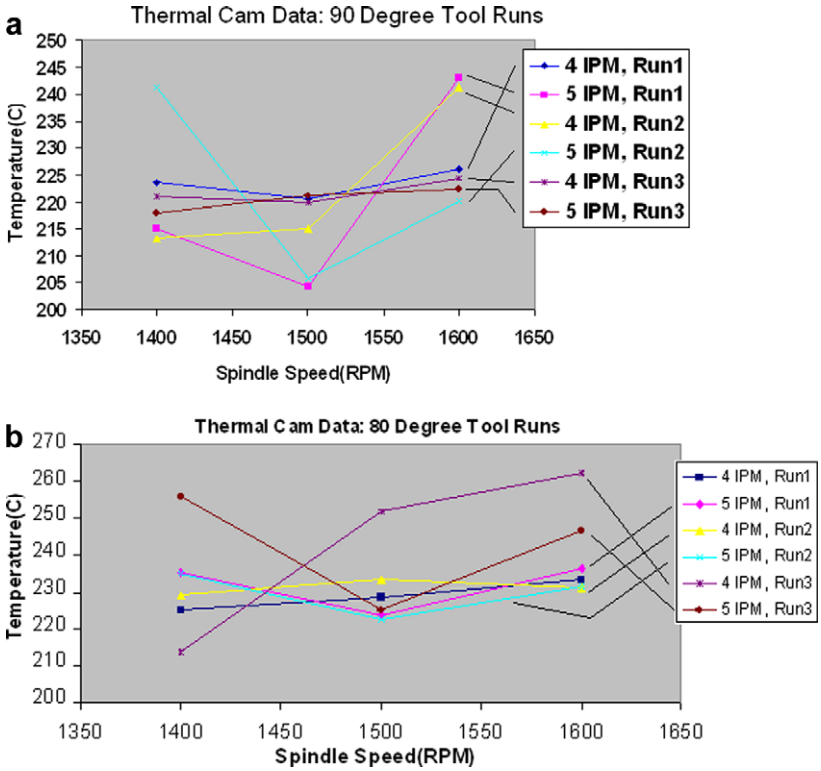

Fig. 9. (a)Thermal camera data for 90° tool runs and (b) Thermal camera data for 80° tool runs.

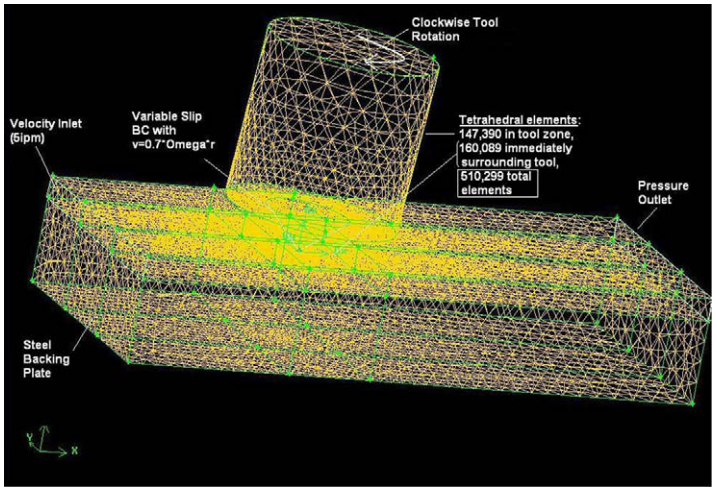

Fig. 10. CFD model geometry consisting of 510,299 tetrahedral elements.

tion rates, spindle speeds, and traverse rates. The cone tip tends to drag through the material towards the end of the retraction when probe surface area, probe tangential velocity, heat, and pressure are insufficient for proper FSW consolidation. Pin tapered retraction from a full penetration weld is likely achievable with an aggressive increase in spindle speed as the tool retracts. A shallow dimple in the material surface would however be difficult to eliminate. Application to variable depth welding and open-loop control welding are trivial tasks. From this experiment it can be concluded that a conical FSW tool could produce high quality, full penetration welds without the assistance of force control in materials which vary in thickness over their length.

Acknowledgements

Completion of this work was made possible by a research license from the Edison Welding Institute (EWI) for use of a Variable Penetration Tool (VPT). This work was funded by the NASA Space Grant Consortium of Tennesse and by Vanderbilt University. The authors would like to thank Kate Lunsford and UTSI for assistance in etching and microscopy. The authors would like to thank Bob Patchin and John Fellenstein for assistance in the design and machining of tools and fixturing. In addition, the authors would like to acknowledge valuable advice and expertise provided by Jeff Bernath and Michelle Laverty of EWI.

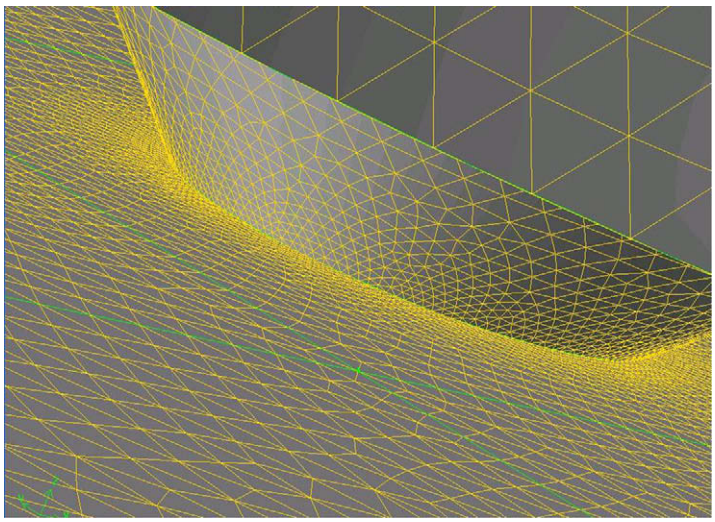

Fig. 11. Increasing element refinement towards the weld interface.

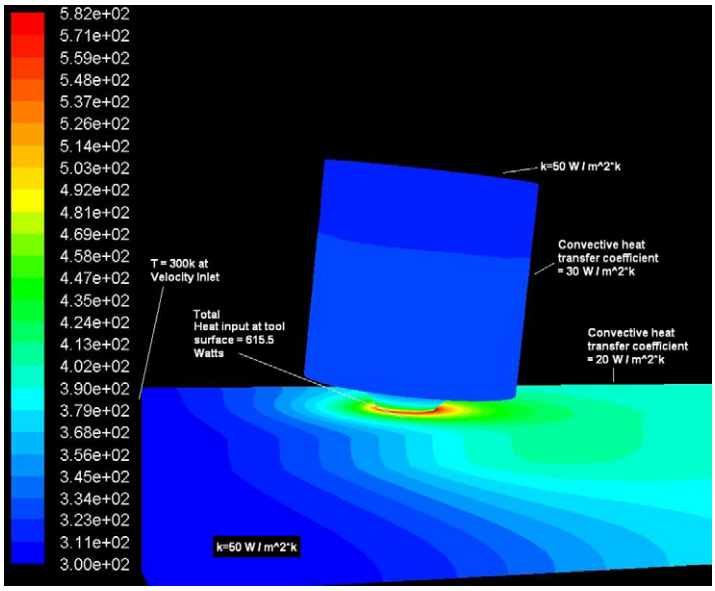

Fig. 12. Thermal boundary conditions used in the model.

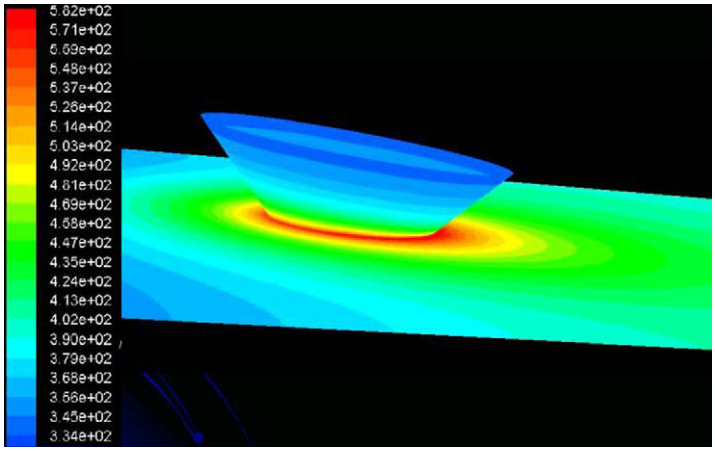

Fig. 13. Temperature gradients in the vicinity of the weld interface.

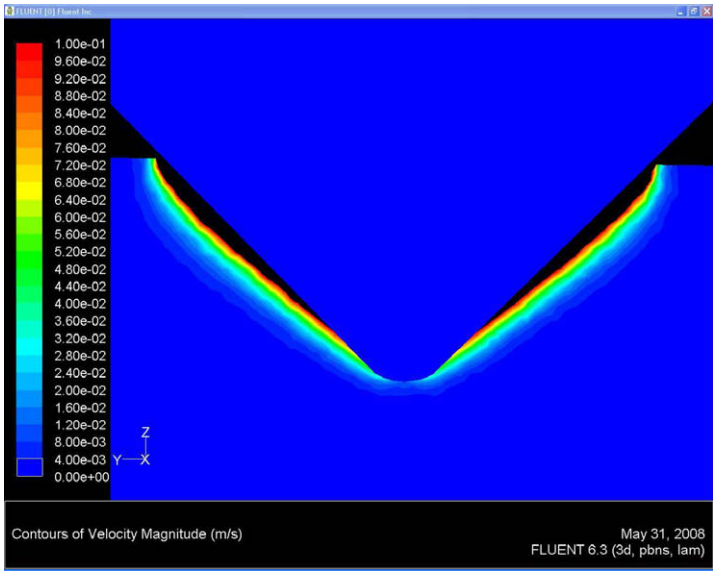

Fig. 14. Lateral cross-section of the weld model showing contours of velocity magnitude in the material surrounding the tool. This outlines the so-called thermo-mechanically affected zone (TMAZ). The blackened area in the vicinity of the tool is outside the scale of this particular contour graph, which has been cropped to accentuate flow near the TMAZ boundary.

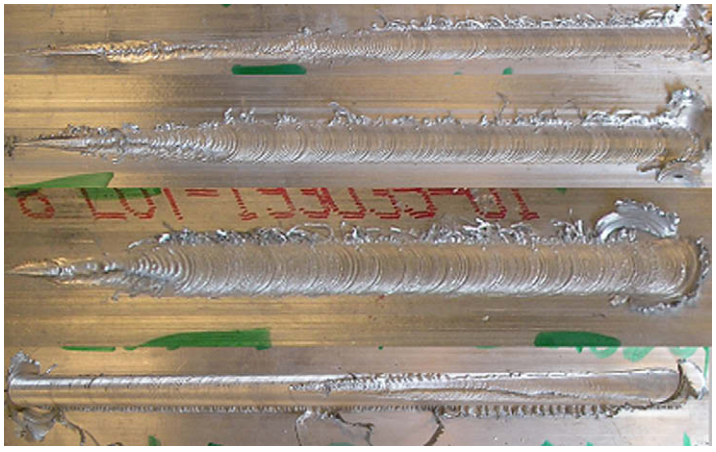

Fig. 15. Attempts a probe tapered retraction from 1/8 in. material full penetration welds at various parameters. The probe tends to 'drag' through the material near exit.

References

[1] Trapp T, Fischer J, Bernath J. Edison Welding Institute (ESI). US Patent #7,234,626.

[2] Bernath J. Friction stir welding technology engineering team leader. Edison Welding Institute (ESI). Personal communication; November 10, 2008.

[3] Ding J. The hydraulic controlled auto-adjustable pin tool for friction stir welding. The US Government through the National Aeronautics and Space Administration. US Patent #5,893,507; 1996.

[4] Sheppard T, Wright D. Determination of flow stress: Part 1 constitutive equation for aluminum alloys at elevated temperatures. Met Technol 1979;6(June):215–23.

[5] Sellars CM, Tegart WJM. Hot workability. Int Metall Rev 1972;17:1–24.

[6] Simar A, Pardoen T, de Meester B. Influence of friction stir welding parameters on the power input and temperature distribution on friction stir welding. In: Proceedings of the 5th international symposium on friction stir welding; 2004.

[7] Simar A, Pardoen T, de Meester B. Effect of rotational material flow on temperature distribution in friction stir welds. Sci Technol Weld Join 2007;12(4):324.

[8] Santiago DH, Lombera G, Santiago U. Numerical modeling of welded joints by the friction stir welding process. Mater Res 2004;7(4):569.

[9] Pew JW, Nelson TW, Sorensen CD. Torque based weld power model for friction stir welding. Sci Technol Weld Join 2007;12(4):341.

[10] Colegrove P, Painter M, Graham D, Miller T. 3 Dimensional flow and thermal modelling of the friction stir welding process. In: Proceedings of the 2nd international symposium on friction stir welding; 2001.

[11] Linder K, Khandahar Z, Khan J, Tang W, Reynolds AP. Rationalization of hardness distribution in alloy 7050 friction stir welds based on weld energy, weld power, and time/temperature history. In: Proceedings of the 6th international symposium on friction stir welding; 2007.

[12] Dickerson TL, Shi Q-Y, Shercliff HR. Heat flow into friction stir welding tools. In: Proceedings of the 4th international symposium on friction stir welding; 2003.

[13] Nunes AC, Bernstien EL, McClure JC. A rotating plug model for friction stir welding. In: Proceedings of the 81st American Welding Society annual convention, Chicago (IL); 2000.

[14] St-Georges L, Dasylva-Raymond V, Kiss LI, Perron AL. Prediction of optimal parameters of friction stir welding. In: Proceedings of the 6th international symposium on friction stir welding; 2007.

[15] Chao YJ, Qi X. Heat transfer and thermo-mechanical analysis of friction stir joining of AA6061-T6 plates. In: Proceedings of the 1st international symposium on friction stir welding; 1999.

[16] Liechty BC, Webb BW. Modeling the frictional boundary conditions in friction stir welding. Int J Mach Tools Manufact 2008. doi:10.1016/j.ijmachtools.2008.04.005.